

Mesoporous Silica-Coated Hollow Manganese Oxide Nanoparticles as Positive T_1 Contrast Agents for Labeling and MRI Tracking of Adipose-Derived Mesenchymal Stem Cells

Taeho Kim,^{†,‡,§} Eric Momin,^{||} Jonghoon Choi,^{†,‡} Kristy Yuan,^{||} Hasan Zaidi,^{||} Jaeyun Kim,^{†,‡,§} Mihyun Park,[§] Nohyun Lee,[§] Michael T. McMahon,^{†,⊥} Alfredo Quinones-Hinojosa,^{||} Jeff W. M. Bulte,^{†,‡,¶,#} Taeghwan Hyeon,^{*,§} and Assaf A. Gilad^{*,†,‡,⊥}

[†]Russell H. Morgan Department of Radiology and Radiological Science, Division of MR Research, The Johns Hopkins University School of Medicine, Baltimore, Maryland 21205, United States

[‡]Cellular Imaging Section, Institute for Cell Engineering, The Johns Hopkins University School of Medicine, Baltimore, Maryland 21205, United States

[§]National Creative Research Initiative Center for Oxide Nanocrystalline Materials, World Class University program of Chemical Convergence for Energy and Environment, and School of Chemical and Biological Engineering, Seoul National University, Seoul 151-744, Korea

^{||}Department of Neurological Surgery, The Johns Hopkins University School of Medicine, Baltimore, Maryland 21205, United States

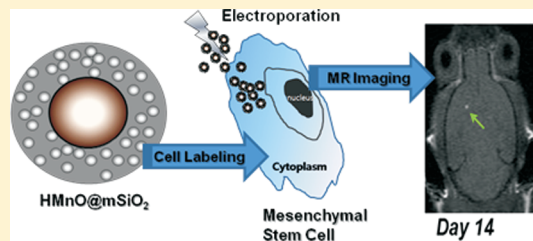
[⊥]F.M. Kirby Research Center for Functional Brain Imaging, Kennedy Krieger Institute, Baltimore, Maryland 21205, United States

[¶]Department of Biomedical Engineering, The Johns Hopkins University School of Medicine, Baltimore, Maryland 21205, United States

[#]Department of Chemical and Biomolecular Engineering, The Johns Hopkins University School of Medicine, Baltimore, Maryland 21205, United States

 Supporting Information

ABSTRACT: Mesoporous silica-coated hollow manganese oxide ($\text{HMnO}@\text{mSiO}_2$) nanoparticles were developed as a novel T_1 magnetic resonance imaging (MRI) contrast agent. We hypothesized that the mesoporous structure of the nanoparticle shell enables optimal access of water molecules to the magnetic core, and consequently, an effective longitudinal (R_1) relaxation enhancement of water protons, which value was measured to be $0.99 (\text{mM}^{-1}\text{s}^{-1})$ at 11.7 T . Adipose-derived mesenchymal stem cells (MSCs) were efficiently labeled using electroporation, with much shorter T_1 values as compared to direct incubation without electroporation, which was also evidenced by signal enhancement on T_1 -weighted MR images in vitro. Intracranial grafting of $\text{HMnO}@\text{mSiO}_2$ -labeled MSCs enabled serial MR monitoring of cell transplants over 14 days. These novel nanoparticles may extend the arsenal of currently available nanoparticle MR contrast agents by providing positive contrast on T_1 -weighted images at high magnetic field strengths.



INTRODUCTION

In recent years, the use of nanoparticles for biomedical imaging has revolutionized the ability to monitor molecular and cellular events in living organisms. Semiconductor nanoparticles (quantum dots) have been applied as fluorescence probes for cell labeling in optical imaging.^{1–3} Gold nanoparticles have been investigated in optical imaging and as biomedical sensors because of their unique optical and electrical properties.^{4,5} Magnetic nanoparticles have also been used as contrast enhancement agents for magnetic resonance imaging (MRI), and as biosensors.^{6–12} MRI is currently one of the most powerful and widely used imaging modalities that provides high spatial resolution combined with excellent anatomical details.^{13–15}

In the past decade, superparamagnetic iron oxide nanoparticles (SPIO) have become the preferred technique for MRI cell tracking,^{16–21} and have now entered the clinical arena.^{22,23}

SPIO-labeled cells have much shorter transverse (T_2) relaxation time and thus, produce hypointensities (dark regions) on T_2/T_2^* -weighted MR images, which presumably indicate the location of the transplanted cells. Unfortunately, SPIO-labeled cells cannot be distinguished from other hypointense regions, such as hemorrhage and blood clots, which are common in many lesions. Therefore, alternative tracking methods using “positive” contrast agents have been explored, i.e. gadolinium (Gd)-based complexes that can generate hyperintense regions as a result of their predominant effects on the longitudinal (T_1) relaxation time of water protons in tissue.^{24–30} Unfortunately, gadolinium-based contrast agents are now associated with nephrogenic systemic fibrosis (NSF), which makes them less favorable agents,³¹ in particular when being retained in cells without rapid clearance

Received: September 21, 2010

Published: February 11, 2011

from the body. A different approach to enhance MRI contrast is to use manganese as a T_1 relaxation agent. Manganese has been mostly used in the form of $MnCl_2$ to study the structure and function of normal or diseased brain.^{32–34} $MnCl_2$ was used for direct labeling of cells *in vitro*.³⁵ Mn has also been chelated and conjugated to proteins to achieve a higher r_1 relaxivity.³⁶ Relaxivity (r_1 , for longitudinal relaxation) describes the change in the relaxation rates of the water protons in the presence of a given contrast agent. Contrast agents with high r_1 values enable lower concentrations of the agent, and consequently, result in higher sensitivity.^{25,36} Alternatively, the longitudinal relaxation can be improved by increasing the number of Mn atoms per particle that can exchange with the water protons, as in the case of nanoparticles. Indeed, manganese oxide (MnO) nanoparticles have recently been explored as a new T_1 MR contrast agent that can delineate fine anatomical features in mouse brain,³⁷ and to track cells with positive contrast.³⁸ However, most of the reported manganese oxide nanoparticles provide weak contrast, and the duration of signal is too short for long-term *in vivo* MR contrast enhancement.^{37–39}

Coating of nanoparticles can significantly improve their stability, biocompatibility, and relaxivity.^{3,16,21,39} Silica has been recognized as a good candidate for a coating material because it is relatively biocompatible and resistant to biodegradation.^{40–44} In particular, mesoporous silica material is an excellent candidate due to its stability in aqueous solution and high labeling efficiency.^{45–53} Furthermore, mesoporous silica allows easy access for water molecules to the magnetic center, which significantly improves the water proton relaxation.^{54,55} In this study, we report on a novel design of MnO nanoparticles that have a 'hollow' MnO core structure and a coating consisting of mesoporous silica (termed HMnO@mSiO₂). The high surface area-to-volume ratio and water accessibility through the pores allows for an efficient T_1 MR contrast agent. This was demonstrated *in vitro* and *in vivo* after labeling of multipotent adipose-derived mesenchymal stem cells (MSCs) with HMnO@mSiO₂ nanoparticles.

■ EXPERIMENTAL SECTION

Synthesis of HMnO@mSiO₂ Nanoparticles. Mesoporous silica-coated MnO nanoparticles were prepared using the following procedure. First, uniformly sized 15 nm MnO nanoparticles were synthesized by the thermal decomposition of Mn-oleate complex.⁵⁶ The resulting MnO nanoparticles stabilized with oleic acid were dispersed in chloroform at a concentration of 10.8 mg Mn/mL, as measured by inductively coupled plasma atomic emission spectroscopy (ICP-AES). A typical mesoporous silica coating onto MnO nanoparticles (MnO@mSiO₂) was performed using a sol–gel reaction of tetraethyl orthosilicate (TEOS) in an aqueous solution containing cetyltrimethylammonium bromide (CTAB) and MnO nanoparticles stabilized with oleic acid.⁴⁹ First, 600 μ L of MnO nanoparticles in chloroform was poured into 5 mL of 0.05 M aqueous CTAB solution and the resulting solution was stirred for 1 h. Forming an oil-in-water microemulsion, the mixture was heated up to 60 °C and maintained at that temperature for 20 min under stirring in order to evaporate the chloroform. The transparent resulting solution of MnO/CTAB was added to a mixture of 25 mL of water and 1.8 mL of 2 M NaOH solution, and the mixture was heated. At approximately 70 °C under stirring, 0.3 mL of TEOS and 1.8 mL of ethylacetate were added to the reaction solution in sequence. The reaction was continued for 12 h at approximately 70 °C. The washing steps for MnO@mSiO₂ nanoparticles with ethanol were performed to remove unreacted species, and then the nanoparticles were redispersed in 5 mL of ethanol.

For the hollow core structure of mesoporous silica-coated MnO nanoparticles, an etching process was performed: 100 μ L of mild hydrochloric acid solution (4%) ($pH \approx 2.4$) was added to the dispersion followed by stirring for 1 h at 70 °C. Acid-etched HMnO@mSiO₂ nanoparticles were then dispersed in 5 mL ethanol. After washing with ethanol two more times, nanoparticles were redispersed in distilled water. After filtration through a 450 nm (pore size) cellulose acetate filter, HMnO@mSiO₂ nanoparticles were finally redispersed in phosphate buffered saline (PBS) (10 mM phosphate, 138 mM NaCl, pH = 7.4) solution.

Relaxivity Measurements. MRI of phantoms was performed using an 11.7 T Bruker Avance system equipped with a 15 mm birdcage RF coil. T_1 and T_2 relaxation times were measured using a modified multiecho spin echo (MSME) protocol.³⁸ Typical settings for T_1 measurements were as follows: 64 × 64 matrix size; echo time (TE) = 6.4 ms; and a repetition time (TR) series of 0.2, 0.4, 0.8, 1, 1.5, 3, 4, 6, and 10 s; and 2 averages per measurement. For T_2 measurements, the parameters were 128 × 128 matrix; 3000 ms repetition time; echo time series of 6.4, 12.8, 19.2, 25.6, 32.0, 38.4, 44.8, 51.2, 57.6, 64.0, 70.4, and 76.8 ms; and 2 averages per measurement. Data processing was performed using Matlab (Mathworks, Natick, MA).

Cell Labeling and Phantom Preparation. Electroporation was used to label cells with HMnO@mSiO₂ nanoparticles. Mouse MSCs were cultured in 80 cm² flasks overnight to 80–90% confluence. On the next day, cells were suspended using trypsin-ethylene diamine tetraacetic acid (EDTA), washed with PBS, and counted. Cells were resuspended and transferred to sterile 0.4 cm gap electroporation cuvettes (Gene Pulser; Bio-Rad). Each cuvette contained 2 × 10⁶ cells suspended in 580 μ L. Nanoparticles dispersed in PBS were added to the cuvette with a final volume of 700 μ L. Cuvettes were kept on ice for one min, and cells were electroporated using a BTX electroporation system (ECM830; Harvard Apparatus). The following electroporation conditions were used: pulse strength = 100 V; N pulses = 5; pulse duration = 5 ms; and pulse interval = 100 ms. After 30 s, cells were transferred to ice for 2 min, suspended in culture medium, transferred to six-well plates. At 24 h following electroporation, cells were washed twice with PBS, harvested using trypsin-EDTA, and counted. For gelatin phantoms, 2 × 10⁶ cells suspended in 50 μ L of PBS were transferred to 0.5 mL polypropylene tubes and mixed with 50 μ L of 10% gelatin in PBS. The final cell concentration was 2 × 10⁴ cells/ μ L in 5% gelatin.

Cellular Imaging in Vitro. A solution of 2 × 10⁶ MSCs suspended in 580 μ L PBS was mixed with 120 μ L HMnO@mSiO₂ (or PBS as a control) and electroporated or incubated. MRI scans of *in vitro* phantoms were obtained using a Bruker 9.4 T MRI scanner. T_1 relaxation was measured using an MSME pulse sequence (for T_1 ; TE = 9 ms, and TR = 0.2, 0.3, 0.5, 0.8, 1, 1.5, 2, 4, 6, and 10 s). Data processing was performed using Matlab (Mathworks, Natick, MA).

Cellular Imaging in Vivo. Animal experiments were performed in accordance with a protocol approved by Animal Care and Use Committee of the Johns Hopkins University School of Medicine. C15/BL6 male mice (weighing 20 g) were anesthetized with ketamine/xylazine (100/15 mg per kg), and positioned in a stereotaxic device (Stoelting, Wood Dale, IL, U.S.A.). A small skin incision was made in the midline to expose the skull. Using a motorized nanoinjector (Stoelting, Inc.) and 10 μ L Hamilton syringe (Hamilton, Reno, NV, U.S.A.) with an attached 33G needle, 1.0 × 10⁵ labeled or unlabeled MSCs were injected into the putamen of mice ($n = 2$), according to the following coordinates from bregma: anteroposterior [AP] = 1.5 mm; mediolateral [ML] = 1.34 mm; and dorsoventral [DV] = -3.5 mm. Cells were injected slowly over 4 min, and the needle was left in place for 1 min before being withdrawn. The incision was closed with surgical glue, and postoperative analgesia was provided with Ketofen (2 mg/kg) for 72 h.

Serial *in vivo* MRI scans were performed on a Bruker 9.4 T horizontal bore magnet, equipped with a 30-mm Sawtooth resonator (Bruker), and

Scheme 1. Schematic Illustration of the Synthesis of HMnO@mSiO₂ Nanoparticles and Labeling of MSCs

using an MSME pulse sequence. For T_1 measurements, the following parameters were used: TE = 10.5 ms; TR = 1.5 s; FOV = 2.1 × 2.1 cm; and matrix size = 256 × 96.

RESULTS AND DISCUSSION

Synthesis and Characterization of HMnO@mSiO₂ Nanoparticles. Scheme 1 describes the synthesis of HMnO@mSiO₂ nanoparticles and labeling of MSCs using electroporation. Manganese oxide nanoparticles with a mean diameter of 15 nm, stabilized with oleic acid, were synthesized by the thermal decomposition of manganese oleate complex.⁵⁶ Then, mesoporous silica shells were coated with a silica sol–gel reaction of tetraethyl orthosilicate (TEOS) in aqueous solution containing cetyltrimethylammonium bromide (CTAB) and MnO nanoparticles under basic conditions.⁴⁹ Hydrophobic MnO nanoparticles capped with oleic acid were transferred to aqueous solution using CTAB, and the subsequent formation of a mesoporous silica shell was achieved. CTAB molecules were used not only as the stabilizing agent to transfer hydrophobic nanoparticles to the aqueous phase, but also as the organic structure-directing template to establish mesopores on the silica shell. The creation of the hollow interior of the MnO cores, along with template removal, was achieved by acid etching and refluxing in ethanol solutions (pH ≈ 2.4). TEM revealed discrete and uniformly sized HMnO@mSiO₂ nanoparticles. The average diameter of the particles was about 65 nm and the MnO core size was 15 nm. The nanoparticles were all well-dispersed and separated from one another. The mesoporous silica shell and hollow MnO core structures can be clearly seen on the TEM (Figure 1a) and HRTEM (Figure 1b) images. We also confirmed the mesoporous structures of HMnO@mSiO₂ nanoparticles using N₂ adsorption/desorption isotherms. The average pore diameter calculated using the Barrett–Joiner–Halenda (BJH) method was 3.3 nm. The Brunauer–Emmett–Teller (BET) surface area and pore volume of the HMnO@mSiO₂ nanoparticles were measured to be 181.3 m² g⁻¹ and 0.38 cm³ g⁻¹ (Figure S1, Supporting Information), respectively. These BET results indicate that HMnO@mSiO₂ nanoparticles are highly porous and have large surface area, which enables rapid access for water molecules to the manganese core through the nanopores of the particles. In addition, the hollow interior of the MnO cores also enables more Mn ions to be exposed to water molecules at the inner surface.⁵⁷ HMnO@mSiO₂ nanoparticles that have a large surface area at the manganese center resulting from these novel structures can be expected to have high T_1 relaxivities.

The MRI properties of the HMnO@mSiO₂ nanoparticles in water were characterized using an 11.7 T MR scanner. The

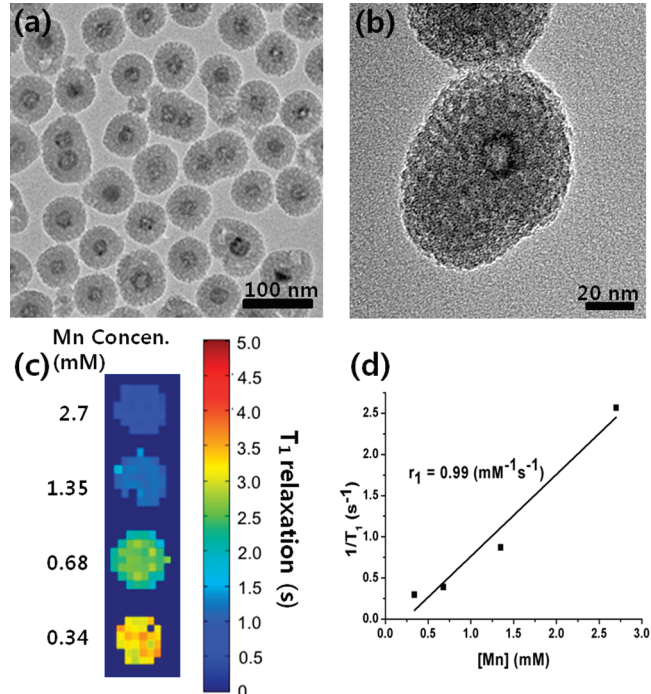


Figure 1. Characterization of HMnO@mSiO₂ nanoparticles. (a) TEM image. (b) HRTEM image of a single nanoparticle. (c) T_1 map of HMnO@mSiO₂ nanoparticles suspended in water at 11.7 T. (d) Plot of $1/T_1$ versus Mn concentration. The slope indicates the specific relaxivity (r_1).

paramagnetic nanoparticles shortened the T_1 of water protons significantly (Figure 1c). The molar relaxivity (effectiveness as contrast agent) was obtained by measuring the relaxation rate with increasing concentrations of nanoparticles (Figure 1c), and was calculated to be 0.99 mM⁻¹ s⁻¹ (Figure 1d). This relaxivity is significantly higher as compared to that measured for MnO nanoparticles encapsulated with PEG-phospholipids (MnO@PEG-phospholipid),^{37,38} dense silica-coated MnO nanoparticles (MnO@dSiO₂)³⁹ (Figure S2, Supporting Information), and nonetched mesoporous silica-coated MnO nanoparticles (MnO@mSiO₂). Summarized in Table 1, the r_1 values of HMnO@mSiO₂ nanoparticles were 12.4, 9.0, and 1.5 times higher than those of the MnO@dSiO₂, MnO@PEG-phospholipid, and MnO@mSiO₂ nanoparticles, respectively. These findings suggest that the majority of the improvement over other nanoparticles is derived from the coating, consistent with our hypothesis that the

Table 1. Relaxivity Data of Manganese Oxide-Based Nanoparticles (per Mn)

nanoparticles ^a	r_1 ($\text{mM}^{-1} \text{s}^{-1}$)	r_2 ($\text{mM}^{-1} \text{s}^{-1}$)	r_2/r_1	field (T)	ref
HMnO@mSiO ₂	0.99	11.02	11.13	11.7	this paper
MnO@PEG-phospholipid	0.11	6.16	56	11.7	this paper
MnO@mSiO ₂	0.65	9.50	14.61	11.7	this paper
MnO@dSiO ₂	0.08	2.27	28.37	11.7	this paper
HMnO@mSiO ₂	1.72	11.30	6.56	1.5	this paper
WMON	0.21	1.49	7.09	3	57
HMON	1.42	7.74	5.45	3	57
Mn-NMOFs	4.0	112.8	28.2	9.4	60
Mn ₃ O ₄ @SiO ₂ (RBTC)	0.47	N/A		3.0	39
HAS-MNOP	1.97	N/A		7.0	61

^a Nanoparticle annotations: HMnO@mSiO₂ - mesoporous silica-coated, hollow MnO nanoparticles. MnO@PEG-phospholipid - MnO nanoparticles encapsulated with PEG-phospholipid. MnO@mSiO₂ - nonetched mesoporous silica-coated MnO nanoparticles. MnO@dSiO₂ - dense silica-coated MnO nanoparticles. WMON - water-dispersible manganese oxide nanoparticles. HMON - hollow manganese oxide nanoparticles. Mn-NMOFs - manganese-containing nanoscale metal-organic frameworks (NMOFs). HAS-MNOP - human serum albumin-coated manganese oxide nanoparticles.

mesoporous shell allows better water exchange with the MnO core. Water diffusion across mesoporous silica has been studied previously using pulsed field gradient (PFG) diffusion NMR.⁵⁸ It was shown that water diffuses anisotropically inside mesoporous silica in comparison to isotropic diffusion in the surrounding environment, with the fastest diffusion component occurring along the channels in the mesoporous silica. The existence of nanopores allows water diffusion to the manganese core leading to efficient relaxation of water in the vicinity of the nanoparticles. In fact, using PFG NMR and magic angle spinning NMR, similar diffusion properties were shown for larger molecules such as pentane, cyclohexane, *n*-dodecane, and amino acids such as alanine.⁵⁹ An additional improvement over MnO@mSiO₂ (1.5 fold, see above) may be a result of the acidic etching, which increases the surface area-to-volume ratio, and further increases the exchange of the water with Mn²⁺ ions. This improvement is in agreement with previously reported relaxivity for hollow manganese oxide nanoparticles.⁵⁷ Recent reports on other manganese-based nanoparticles describe wide range of relaxivity (r_1) values.^{39,57,60,61} It is difficult to compare the relaxivities of those nanoparticles since the relaxivity was measured at different field strengths (Table 1). When measured at lower field (1.5 T), the HMnO@mSiO₂ nanoparticles gave higher r_1 but similar r_2 values ($r_1 = 1.72 \text{ mM}^{-1} \text{s}^{-1}$, $r_2 = 11.30 \text{ mM}^{-1} \text{s}^{-1}$) in comparison to those measured at 11.7 T. As expected, the r_2/r_1 ratio at lower field is lower. The closer this ratio is to 1, the better the nanoparticle will function as “positive” contrast agent. For example, “Magnevist” (a commercial gadolinium complex) has an optimal r_2/r_1 ratio of 1 ($r_1 = 4.6 \text{ mM}^{-1} \text{s}^{-1}$, $r_2 = 4.5 \text{ mM}^{-1} \text{s}^{-1}$) at 1.5 T,⁶² in comparison to 6.56 for HMnO@mSiO₂ at the same field strength. When compared to manganese compounds^{33,36} such as MnCl₂ and chelated manganese, the HMnO@mSiO₂ nanoparticles have lower relaxivity. Nevertheless, the nanoparticles were designed specifically for cell labeling and tracking which is not possible with these compounds, even if the relaxivity had to be compromised.

The X-ray diffraction (XRD) pattern (Figure S3, Supporting Information) revealed polycrystalline properties of the HMnO@mSiO₂ nanoparticles, consisting mainly of tetragonal Mn₃O₄ phase and small fraction of cubic MnO phase. The existence of an amorphous silica shell also contributes to the broad peaks of the patterns. In particular, it was found that the crystallinity of the nanoparticle was decreased after the acid etching. The dissolution of the cubic MnO phase from the core part was also examined. After acid etching, HMnO@mSiO₂ nanoparticles were mainly composed of the tetragonal Mn₃O₄ phase.

HMnO@mSiO₂ nanoparticles are stable in water and PBS solution for over a month. The hydrodynamic diameter of HMnO@mSiO₂ nanoparticles in PBS solution was measured to be 86 nm using Dynamic Light Scattering (Figure S4, Supporting Information). This demonstrates that nanoparticles are stable in PBS and do not form aggregates, which is desirable for its use as intracellular labeling agent. This good colloidal stability of the HMnO@mSiO₂ nanoparticles results from the negative charge of the silica surface. As shown by zeta potential (ζ) measurements (Figure S5, Supporting Information), the surface potential of the HMnO@mSiO₂ nanoparticles was -30.43 (mV) in PBS (10 mM phosphate, 138 mM NaCl, pH = 7.4) solution.

Cellular Uptake and in Vitro MRI. In order to assess the feasibility of HMnO@mSiO₂ nanoparticles for cell labeling, we initially evaluated the cellular uptake in vitro. In this study, we have chosen to use multipotent mesenchymal stem cells (MSCs), which possess the ability to migrate to sites of tissue injury, have many possible therapeutic applications, including the replacement of damaged tissue and the treatment of cancer.^{63–65} Successful clinical translation for the application of MSCs requires an imaging modality that noninvasively permits their visualization and localization in a living organism. Mouse adipose-derived MSCs were labeled using either electroporation or a simple incubation approach. Electroporation uses an electrical pulse to induce a change in the electrochemical permeability of the cell membrane and enables efficient intracytoplasmic labeling of cells.⁶⁶ This approach is commonly used for transferring DNA and chemotherapeutic drugs into cells, and was recently applied to cell labeling with superparamagnetic iron oxide nanoparticles (SPIO)⁶⁷ and MnO nanoparticles.³⁸ We hypothesized that electroporation could also be efficiently used for cell labeling with HMnO@mSiO₂ nanoparticles. Since the cell membrane is negatively charged,⁶⁸ the negative charge of the nanoparticle would result in repulsion of the nanoparticles by the cell membrane, and thus, uptake would be hampered. However, with electroporation, negatively charged HMnO@mSiO₂ nanoparticles can be effectively introduced into cells without using other transfection agents, such as cationic, positively charged molecules.⁶⁹

Figure 2a shows a T_1 -weighted MR image of tubes containing MSCs electroporated with different concentrations of HMnO@mSiO₂ nanoparticles suspended in 5% gelatin. The higher the nanoparticle concentration used for labeling, the brighter the tube appeared on the image. Figure 2b demonstrates that electroporation

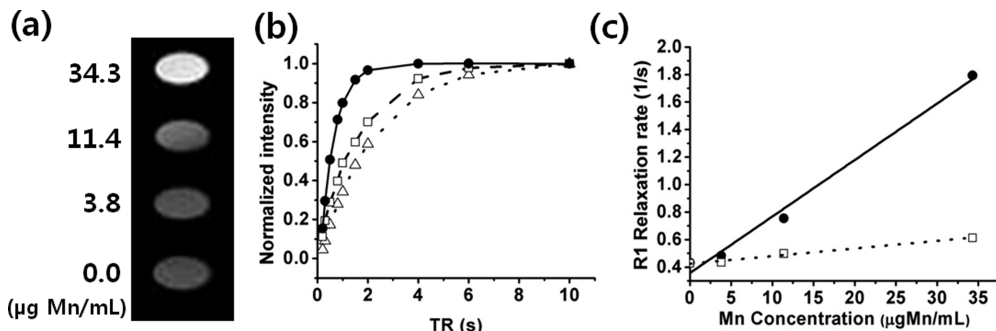


Figure 2. (a) T_1 -weighted MR image of adipose derived MSCs suspended in 5% gelatin. The cells in each tube were electroporated with HMnO@mSiO₂ nanoparticles (0–34.3 μg Mn/mL). (b) Normalized MRI signal intensity of cells electroporated with nanoparticles (34.3 μg Mn/mL) (●), incubated with nanoparticles (34.3 μg Mn/mL) (□), or electroporated without nanoparticles (△). (c) The R_1 relaxation rate plotted as a function of the nanoparticle concentration used for labeling the cells (electroporation (●), incubation (□)).

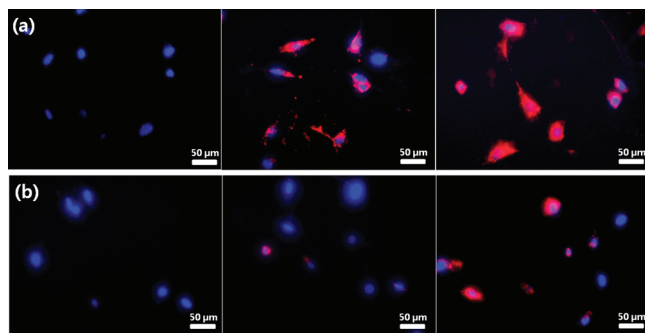


Figure 3. Fluorescence microscopy images of RITC-HMnO@mSiO₂-labeled MSCs, counterstained with Hoechst 33342. Using (a) electroporation or (b) simple incubation with nanoparticles (0, 11.4, and 34.3 μg Mn/mL) (left to right). Cellular uptake of nanoparticles was dose-dependent. Higher nanoparticle uptake was observed in electroporated MSCs.

with nanoparticles shortens T_1 much more efficiently than direct incubation of the cells with the nanoparticles. Figure 2c shows the linear correlation between the relaxation rate ($R_1 = 1/T_1$) and the concentration of nanoparticles that was used to label the cells, both by electroporation ($R^2 = 0.994$) and by incubation ($R^2 = 0.989$). At higher nanoparticle concentration, the electroporation is much more efficient than incubation. For these samples, the manganese ion content was measured using ICP measurement. The Mn concentration was 9.0 μg Mn/mL (= 0.35 pg Mn/cell) and 1.8 μg Mn/mL (= 0.09 pg Mn/cell) for phantom of MSCs labeled with electroporation and incubation, respectively. These findings indicate that 26.23% and 5.24% of the added nanoparticles were taken up by MSCs using electroporation and incubation, respectively. Next, both cellular labeling using electroporation and simple incubation were investigated using nanoparticles conjugated with rhodamine B isothiocyanate (RITC) (Figure 3). This fluorescent organic dye could be easily conjugated to the silica surface using simple silane conjugation chemistry, as previously reported.^{42,49,70,71} For the same nanoparticle concentration, MSCs labeled with electroporation (Figure 3a) showed a higher uptake of nanoparticles than MSCs labeled with incubation (Figure 3b). There was also a clear concentration-dependent cellular uptake of the nanoparticles. As was previously shown, compounds that were introduced into the cells via incubation are more likely to accumulate in endosomes, while with electroporation the compounds are freely distributed within the cytoplasm. This may

also explain in part the lower relaxivity observed for cells incubated with the particles in comparison to electroporation, since with incubation the particles are in confined region (endosome) and have restricted exchange with water in contrast to electroporated nanoparticles.⁷²

Cell Viability and Differentiation of Labeled MSCs. To evaluate the possible cytotoxic effects of the HMnO@mSiO₂ nanoparticles on MSCs, cell viability was assessed with the MTS (3-(4,5-dimethylthiazol-2-yl)-5-(3-carboxymethoxyphenyl)-2-(4-sulfophenyl)-2H-tetrazolium) assay. As shown in Figure S6, high cell viability (more than 75%) was still attained at 24 h after electroporation with HMnO@mSiO₂ nanoparticles at a concentration of 68.6 μg Mn/mL. The effect of electroporation with HMnO@mSiO₂ nanoparticles on the differentiation of adipose-derived MSCs was also studied. It was found that MSCs retained the ability to differentiate into adipocytes; however, differentiation into an osteogenic phenotype could not be induced (Figure S7, Supporting Information). These findings, taken together, indicate that HMnO@mSiO₂ nanoparticles by electroporation have a minimal impact on cell viability, but its effect on cell differentiation should be carefully evaluated for each specific application. In this respect, it is important to note that while SPIOs were reported to inhibit chondrogenesis,⁷³ SPIO-cell tracking clinical studies have nevertheless been initiated.²²

In Vivo MR Imaging. In order to study the feasibility of HMnO@mSiO₂ nanoparticles for long-term in vivo cell tracking, the fate of transplanted, labeled MSCs was serially monitored with MRI. In mice transplanted with unlabeled MSCs, no hyperintensity could be detected (red arrow, Figure 4a). However, in mice transplanted with HMnO@mSiO₂-labeled MSCs, a hyperintense region was observed at the transplantation site (green arrows, Figure 4b). Serial imaging over 14 days demonstrated that the nanoparticles were stable enough to produce sustained contrast in vivo and, therefore, are suitable for monitoring noninvasively the fate of transplanted cells.

The current HMnO@mSiO₂ nanoparticles can be further applied to MRI contrast agents for detecting tumors when conjugated with antibodies³⁷ or RGD peptides⁶⁰ that can be targeted directly to cancer cells or to the tumor vasculature, respectively. Furthermore, stem cells labeled with the HMnO@mSiO₂ nanoparticles can assist in detecting tumors because stem cells tend to migrate into tumor sites.^{74,75} And most importantly, such stem cells can be engineered to perform an antitumor activity.

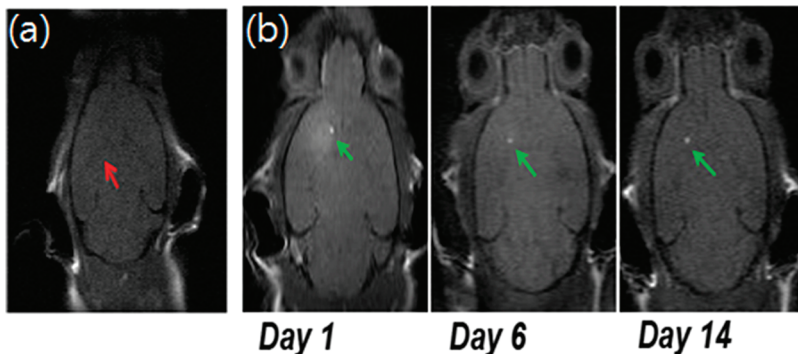


Figure 4. In vivo MRI of transplanted MSCs. (a) No hyperintense signal (red arrow) was detected in mouse transplanted with unlabeled MSCs. (b) Hyperintense signals (green arrows) were detected in mouse transplanted with HMnO@mSiO₂-labeled MSCs and were still visible 14 days after injection.

CONCLUSIONS

In summary, we have synthesized and characterized mesoporous silica-coated hollow manganese oxide nanoparticles. These HMnO@mSiO₂ nanoparticles showed a significantly higher r_1 relaxivity over other existing manganese oxide nanoparticle-based contrast agents. The porous coating, which enables water exchange across the shell, combined with the large surface area-to-volume ratio resulting from the novel structure increases water accessibility to the manganese core and consequently provides enhanced T_1 contrast. These nanoparticles showed high cellular uptake by adipose-derived MSCs, using electroporation, and were detected with MRI both in vitro and intracranially in vivo over a prolonged time period. In light of these findings, HMnO@mSiO₂ nanoparticles have a great potential for MRI cell tracking using positive contrast.

ASSOCIATED CONTENT

Supporting Information. Detailed experimental procedures, N₂ adsorption/desorption isotherm of HMnO@mSiO₂, TEM images of PEG-phospholipid capped MnO nanoparticles and dense silica-coated MnO nanoparticles, XRD pattern, DLS data and zeta potential data of HMnO@mSiO₂ nanoparticles, cell viability data at 24 h after electroporation or incubation with HMnO@mSiO₂ nanoparticles, and differentiation images of MSCs labeled with HMnO@mSiO₂ nanoparticles. This material is available free of charge via the Internet at <http://pubs.acs.org>.

AUTHOR INFORMATION

Corresponding Author

thyeon@snu.ac.kr; assaf.gilad@jhu.edu

ACKNOWLEDGMENT

This work was supported by NIH Grants 1R21EB008769, 5R21NS065284, and 2RO1 NS045062. T.H. acknowledges financial support by the Korean Ministry of Education, Science and Technology through National Creative Research Initiative (R16-2002-003-01001-0), Strategic Research (2010-0029138), and World Class University (R31-10013) Programs of National Research Foundation (NRF) of Korea. This work was also supported, in part, by the NIH Grant 5K08NS055851 and an HHMI grant for A.Q.H., K.Y., and H.Z. as well as the Doris Duke grant for E.M. We thank Segun M. Bernard and Derrick Pyomin Jeon for technical assistance.

REFERENCES

- Dubertret, B.; Skourides, P.; Norris, D. J.; Noireaux, V.; Brivanlou, A. H.; Libchaber, A. *Science* **2002**, 298, 1759.
- Kim, S.; Lim, Y. T.; Soltesz, E. G.; De Grand, A. M.; Lee, J.; Nakayama, A.; Parker, J. A.; Mihaljevic, T.; Laurence, R. G.; Dor, D. M.; Cohn, L. H.; Bawendi, M. G.; Frangioni, J. V. *Nat. Biotechnol.* **2004**, 22, 93.
- Medintz, I. L.; Uyeda, H. T.; Goldman, E. R.; Mattoussi, H. *Nat. Mater.* **2005**, 4, 435.
- Nam, J.-M.; Thaxton, C. S.; Mirkin, C. A. *Science* **2003**, 301, 1884.
- Rosi, N. L.; Mirkin, C. A. *Chem. Rev.* **2005**, 105, 1547.
- Gao, J.; Gu, H.; Xu, B. *Acc. Chem. Res.* **2009**, 42, 1097.
- Jun, Y.-W.; Lee, J.-H.; Cheon, J. *Angew. Chem., Int. Ed.* **2008**, 47, 5122.
- Gao, J.; Xu, B. *Nano Today* **2009**, 4, 37.
- Gao, J.; Liang, C.; Cheung, J. S.; Pan, Y.; Kuang, Y.; Zhao, F.; Zhang, B.; Zhang, X.; Wu, E. X.; Xu, B. *J. Am. Chem. Soc.* **2008**, 130, 11828.
- Xie, J.; Chen, K.; Lee, H.-Y.; Xu, C.; Hsu, A. R.; Peng, S.; Chen, X.; Sun, S. *J. Am. Chem. Soc.* **2008**, 130, 7542.
- Xu, C.; Xie, J.; Ho, D.; Wang, C.; Kohler, N.; Walsh, E. G.; Morgan, J. R.; Chin, Y. E.; Sun, S. *Angew. Chem., Int. Ed.* **2008**, 47, 173.
- Na, H. B.; Song, I. C.; Hyeon, T. *Adv. Mater.* **2009**, 21, 2133.
- Massoud, T. F.; Gambhir, S. S. *Gene Dev.* **2003**, 17, 545.
- Weissleder, R.; Mahmood, U. *Radiology* **2001**, 219, 316.
- Weissleder, R.; Pittet, M. J. *Nature* **2008**, 452, 580.
- Bulte, J. W. M.; Douglas, T.; Witwer, B.; Zhang, S.-C.; Strable, E.; Lewis, B. K.; Zywicke, H.; Miller, B.; van Gelderen, P.; Moskowitz, B. M.; Duncan, I. D.; Frank, J. A. *Nat. Biotechnol.* **2001**, 19, 1141.
- Bulte, J. W. M.; Zhang, S.-C.; van Gelderen, P.; Herynek, V.; Jordan, E. K.; Duncan, I. D.; Frank, J. A. *Proc. Natl. Acad. Sci. U.S.A.* **1999**, 96, 15256.
- Jun, Y.-W.; Huh, Y.-M.; Choi, J.-S.; Lee, J.-H.; Song, H.-T.; Kim, S.; Yoon, S.; Kim, K.-S.; Shin, J.-S.; Suh, J.-S.; Cheon, J. *J. Am. Chem. Soc.* **2005**, 127, 5732.
- Heyn, C.; Ronald, J. A.; Ramadan, S. S.; Snir, J. A.; Barry, A. M.; MacKenzie, L. T.; Mikulis, D. J.; Palmieri, D.; Bronder, J. L.; Steeg, P. S.; Yoneda, T.; MacDonald, I. C.; Chambers, A. F.; Rutt, B. K.; Foster, P. J. *Magn. Reson. Med.* **2006**, 56, 1010.
- Kraitchman, D. L.; Heldman, A. W.; Atalar, E.; Amado, L. C.; Martin, B. J.; Pittenger, M. F.; Hare, J. M.; Bulte, J. W. M. *Circulation* **2003**, 107, 2290.
- Lewin, M.; Carlesso, N.; Tung, C.-H.; Tang, X.-W.; Cory, D.; Scadden, D. T.; Weissleder, R. *Nat. Biotechnol.* **2000**, 18, 410.
- Bulte, J. W. M. *Am. J. Roentgenol.* **2009**, 193, 314.
- de Vries, I. J.; Lesterhuis, W. J.; Barentsz, J. O.; Verdijk, P.; Krieken, J. H.; Boerman, O. C.; Oyen, W. J. G.; Bonenkamp, J. J.; Boezeman, J. B.; Adema, G. J.; Bulte, J. W. M.; Scheenen, T. W. J.; Punt, C. J. A.; Heerschap, A.; Figgdr, C. G. *Nat. Biotechnol.* **2005**, 23, 1407.

- (24) Aime, S.; Castelli, D. D.; Lawson, D.; Terreno, E. *J. Am. Chem. Soc.* **2007**, *129*, 2430.
- (25) Caravan, P. *Chem. Soc. Rev.* **2006**, *35*, 512.
- (26) Caravan, P.; Das, B.; Dumas, S.; Epstein, F. H.; Helm, P. A.; Jacques, V.; Koerner, S.; Kolodziej, A.; Shen, L.; Sun, W.-C.; Zhang, Z. *Angew. Chem., Int. Ed.* **2007**, *46*, 8171.
- (27) Flacke, S.; Fischer, S.; Scott, M. J.; Fuhrhop, R. J.; Allen, J. S.; McLean, M.; Winter, P.; Sicard, G. A.; Gaffney, P. J.; Wickline, S. A.; Lanza, G. M. *Circulation* **2001**, *104*, 1280.
- (28) Modo, M.; Cash, D.; Mellodew, K.; Williams, S. C. R.; Fraser, S. E.; Meade, T. J.; Price, J.; Hodges, H. *NeuroImage* **2002**, *17*, 803.
- (29) Granot, D.; Addadi, Y.; Kalchenko, V.; Harmelin, A.; Kunz-Schughart, L. A.; Neeman, M. *Cancer Res.* **2007**, *67*, 9180.
- (30) Anderson, S. A.; Lee, K. K.; Frank, J. A. *Invest. Radiol.* **2006**, *41*, 332.
- (31) Perez-Rodriguez, J.; Lai, S.; Ehst, B. D.; Fine, D. M.; Bluemke, D. A. *Radiology* **2009**, *250*, 371.
- (32) Pelleg, G.; Bergman, H.; Ben-Hur, T.; Goelman, G. *J. Magn. Reson. Imaging* **2007**, *26*, 863.
- (33) Silva, A. C.; Lee, J. H.; Aoki, I.; Koretsky, A. P. *NMR Biomed.* **2004**, *17*, 532.
- (34) Yu, X.; Wadghiri, Y. Z.; Sanes, D. H.; Turnbull, D. H. *Nat. Neurosci.* **2005**, *8*, 961.
- (35) Aoki, I.; Takahashi, Y.; Chuang, K.-H.; Silva, A. C.; Igarashi, T.; Tanaka, C.; Childs, R. W.; Koretsky, A. P. *NMR Biomed.* **2006**, *19*, 50.
- (36) Troughton, J. S.; Greenfield, M. T.; Greenwood, J. M.; Dumas, S.; Wiethoff, A. J.; Wang, J.; Spiller, M.; McMurry, T. J.; Caravan, P. *Inorg. Chem.* **2004**, *43*, 6313.
- (37) Na, H. B.; Lee, J. H.; An, K.; Park, Y.; Park, M.; Lee, I. S.; Nam, D.-H.; Kim, S. T.; Kim, S.-H.; Kim, S.-W.; Lim, K.-H.; Kim, K.-S.; Kim, S.-O.; Hyeon, T. *Angew. Chem., Int. Ed.* **2007**, *46*, 5397.
- (38) Gilad, A. A.; Walczak, P.; McMahon, M. T.; Na, H. B.; Lee, J. H.; An, K.; Hyeon, T.; van Zijl, P. C. M.; Bulte, J. W. M. *Magn. Reson. Med.* **2008**, *60*, 1.
- (39) Yang, H.; Zhuang, Y.; Hu, H.; Du, X.; Zhang, C.; Shi, X.; Wu, H.; Yang, S. *Adv. Funct. Mater.* **2010**, *20*, 1733.
- (40) Yi, D. K.; Selvan, S. T.; Lee, S. S.; Papaefthymiou, G. C.; Kundaliya, D.; Ying, J. Y. *J. Am. Chem. Soc.* **2005**, *127*, 4990.
- (41) Selvan, S. T.; Patra, P. K.; Ang, C. Y.; Ying, J. Y. *Angew. Chem., Int. Ed.* **2007**, *46*, 2448.
- (42) Yoon, T. J.; Kim, J. S.; Kim, B. G.; Yu, K. N.; Cho, M.-H.; Lee, J.-K. *Angew. Chem., Int. Ed.* **2005**, *44*, 1068.
- (43) Burns, A. A.; Vider, J.; Ow, H.; Herz, E.; Penate-Medina, O.; Baumgart, M.; Larson, S. M.; Wiesner, U.; Bradbury, M. *Nano Lett.* **2009**, *9*, 442.
- (44) Piao, Y.; Burns, A.; Kim, J.; Wiesner, U.; Hyeon, T. *Adv. Funct. Mat.* **2008**, *18*, 3745.
- (45) Ying, J. Y.; Mehnert, C. P.; Wong, M. S. *Angew. Chem., Int. Ed.* **1999**, *38*, 56.
- (46) Wan, Y.; Zhao, D. *Chem. Rev.* **2007**, *107*, 2821.
- (47) Deng, Y.; Qi, D.; Deng, C.; Zhang, X.; Zhao, D. *J. Am. Chem. Soc.* **2008**, *130*, 28.
- (48) Kim, J.; Lee, J. E.; Lee, J.; Yu, J. H.; Kim, B. C.; An, K.; Hwang, Y.; Shin, C.-H.; Park, J.-G.; Kim, J.; Hyeon, T. *J. Am. Chem. Soc.* **2006**, *128*, 688.
- (49) Kim, J.; Kim, H. S.; Lee, N.; Kim, T.; Kim, H.; Yu, T.; Song, I. C.; Moon, W. K.; Hyeon, T. *Angew. Chem., Int. Ed.* **2008**, *47*, 8438.
- (50) Trewyn, B. G.; Slowing, I. I.; Giri, S.; Chen, H.-T.; Lin, V. S.-Y. *Acc. Chem. Res.* **2007**, *40*, 846.
- (51) Lin, Y.-S.; Wu, S.-H.; Hung, Y.; Chou, Y.-H.; Chang, C.; Lin, M.-L.; Tsai, C.-P.; Mou, C.-Y. *Chem. Mater.* **2006**, *18*, 5170.
- (52) Huang, D.-M.; Hung, Y.; Ko, B.-S.; Hsu, S.-C.; Chen, W.-H.; Chien, C.-L.; Tsai, C.-P.; Kuo, C.-T.; Kang, J.-C.; Yang, C.-S.; Mou, C.-Y.; Chen, Y.-C. *FASEB J.* **2005**, *19*, 2014.
- (53) Liu, H.-M.; Wu, S.-H.; Lu, C.-W.; Yao, M.; Hsiao, J.-K.; Hung, Y.; Lin, Y.-S.; Mou, C.-Y.; Yang, C.-S.; Huang, D.-M.; Chen, Y.-C. *Small* **2008**, *4*, 619.
- (54) Kim, J. S.; Rieter, W. J.; Taylor, K. M. L.; An, H.; Lin, W. *J. Am. Chem. Soc.* **2007**, *129*, 8962.
- (55) Taylor, K. M. L.; Kim, J. S.; Rieter, W. J.; An, H.; Lin, W. *J. Am. Chem. Soc.* **2008**, *130*, 2154.
- (56) Park, J.; An, K.; Hwang, Y.; Park, J.-G.; Noh, H.-J.; Kim, J.-Y.; Park, J.-H.; Hwang, N.-M.; Hyeon, T. *Nat. Mater.* **2004**, *3*, 891.
- (57) Shin, J.; Anisur, R. M.; Ko, M. K.; Im, G. H.; Lee, J. H.; Lee, I. S. *Angew. Chem., Int. Ed.* **2009**, *48*, 321.
- (58) Stallmach, F.; Kalrger, J.; Krause, C.; Jeschke, M.; Oberhagemann, U. *J. Am. Chem. Soc.* **2000**, *122*, 9237.
- (59) Amitay-Rosen, T.; Kababaya, S.; Vega, S. *J. Phys. Chem. B* **2009**, *113*, 6267.
- (60) Taylor, K. M. L.; Rieter, W. J.; Lin, W. *J. Am. Chem. Soc.* **2008**, *130*, 14358.
- (61) Huang, H.; Xie, J.; Chen, K.; Bu, L.; Lee, S.; Cheng, Z.; Li, X.; Chen, X. *Chem. Commun.* **2010**, *46*, 6684.
- (62) Seo, W. A.; Lee, J. H.; Sun, X.; Suzuki, Y.; Mann, D.; Liu, Z.; Terashima, M.; Yang, P. C.; McConnell, M. V.; Nishimura, D. G.; Dai, H. *Nat. Mater.* **2006**, *5*, 971.
- (63) Cowan, C. A.; Klimanskaya, I.; McMahon, J.; Atenza, J.; Witmyer, J.; Zucker, J.; Wang, S.; Morton, C. C.; McMahon, A. P.; Powers, D.; Melton, D. A. *Engl. J. Med.* **2004**, *350*, 1353.
- (64) McKay, R. *Nature* **2000**, *406*, 361.
- (65) Pittenger, M. F.; Mackay, A. M.; Beck, S. C.; Jaiswal, R. K.; Douglas, R.; Mosca, J. D.; Moorman, M. A.; Simonetti, D. W.; Craig, S.; Marshak, D. R. *Science* **1999**, *284*, 143.
- (66) Teissie, J.; Eynard, N.; Gabriel, B.; Rols, M. P. *Adv. Drug Delivery Rev.* **1999**, *35*, 3.
- (67) Walczak, P.; Kedziorek, D. A.; Gilad, A. A.; Lin, S.; Bulte, J. W. M. *Magn. Reson. Med.* **2005**, *54*, 769.
- (68) Zhdanov, R. I.; Podobed, O. V.; Vlassov, V. V. *Bioelectrochemistry* **2002**, *58*, 53.
- (69) Gershon, H.; Ghirlando, R.; Guttmann, S. B.; Minsky, A. *Biochemistry* **1993**, *32*, 7143.
- (70) Lee, J. E.; Lee, N.; Kim, H.; Kim, J.; Choi, S. H.; Kim, J. H.; Kim, T.; Song, I. C.; Park, S. P.; Moon, W. K.; Hyeon, T. *J. Am. Chem. Soc.* **2010**, *132*, 552.
- (71) Burns, A.; Ow, H.; Wiesner, U. *Chem. Soc. Rev.* **2006**, *35*, 1028.
- (72) Terreno, E.; Crich, S. G.; Belfiore, S.; Biancone, L.; Cabella, C.; Esposito, G.; Manazza, A. D.; Aime, S. *Magn. Reson. Med.* **2006**, *55*, 419.
- (73) Kostura, L.; Kraitchman, D. L.; Mackay, A. M.; Pittenger, M. F.; Bulte, J. W. M. *NMR Biomed.* **2004**, *17*, 513.
- (74) Arbab, A. S.; Rad, A. M.; Iskander, A. S. M.; Jafari-Khouzani, K.; Brown, S. L.; Churchman, J. L.; Ding, G.; Jiang, Q.; Frank, J. A.; Soltanian-Zadeh, H.; Peck, D. J. *Magn. Reson. Med.* **2007**, *58*, 519.
- (75) Thu, M. S.; Najbauer, J.; Kendall, S. E.; Harutyunyan, I.; Sangalang, N.; Gutova, M.; Metz, M. Z.; Garcia, E.; Frank, R. T.; Kim, S. U.; Moats, R. A.; Aboody, K. S. *PLoS One* **2009**, *4*, e7218.